GABA produced by multiple bone marrow cell types regulates hematopoietic stem and progenitor cells

Cesi Deng (邓策思)[1], Adedamola Elujoba-Bridenstine[1], Ai Tang Song[1], Rylie M. Ceplina[1], Casey J. Ostheimer[1], Molly C. Pellitteri Hahn[2], Cameron O. Scarlett[2], Owen J. Tamplin[1,*]

[1]Department of Cell and Regenerative Biology, School of Medicine and Public Health, University of Wisconsin-Madison, Madison, WI, USA

[2]Analytical Instrumentation Center, School of Pharmacy, University of Wisconsin-Madison, Madison, WI, USA

[*]Corresponding author: tamplin@wisc.edu

Summary

Hematopoietic stem and progenitor cells (HSPCs) maintain homeostasis of the blood system by balancing proliferation and differentiation. Many extrinsic signals in the bone marrow (BM) microenvironment that regulate this balance are still unknown. We report gamma aminobutyric acid (GABA) metabolite produced in the BM as a regulator of HSPCs. Deletion of the glutamate decarboxylase enzymes (Gad1/2) that produce GABA in either B lineages or endothelial cells (ECs) leads to a moderate reduction in BM GABA levels and HSPC number, suggesting both cell types are GABA sources. However, simultaneous blockade of GABA production from both hematopoietic cells and ECs resulted in a greater reduction of both GABA levels and HSPC numbers. Lower GABA levels in the BM altered the gene expression profile of HSPCs, with expression reduced for proliferation-associated genes and increased for B lineage genes. Our findings suggest GABA from multiple sources coordinates to regulate HSPC activity.

25 **Highlights**

26 - GABA is produced by B cells and endothelial cells in the bone marrow
27 - Lower GABA level in the bone marrow reduces HSPC proliferation
28 - Lower GABA level primes HSPCs to upregulate B cell differentiation programs

29

30 **eTOC blurb**

31 Tamplin and colleagues functionally test production of GABA metabolite in the bone marrow
32 microenvironment as a regulator of hematopoietic stem and progenitor cells. Conditional deletion
33 of GAD enzymes in B cells and endothelial cells demonstrated both are sources of GABA. Lower
34 GABA level primed HSPCs to reduce proliferation and upregulate B cell differentiation programs.

35

36 **Introduction**

37 Hematopoietic stem and progenitor cells (HSPCs) replenish the entire blood system throughout
38 life (Pinho and Frenette, 2019). The balance between HSPC proliferation and differentiation is
39 tightly regulated by extrinsic signals in their microenvironment, also known as the niche. In adults,
40 bone marrow (BM) is the primary site of hematopoiesis and is made up of a highly complex array
41 of different niche cell types. Although research has focused on the cytokines, other growth factors,
42 receptor ligands, and adhesion molecules produced by these different niche cells, there are also
43 understudied factors such as metabolites and neurotransmitters that play a role in regulating HSPC
44 activity. For example, peripheral nerves can provide adrenergic signals that act on stromal cells to
45 regulate HSPC mobilization (Méndez-Ferrer et al., 2008), and dopamine can act directly acting on
46 neuroreceptors on the HSPC surface (Liu et al., 2021). The full range of secreted immune
47 metabolites are reviewed elsewhere (Zhang et al., 2022).

48 Gamma amino-butyric acid (GABA) is a major neurotransmitter in the central nervous system.
49 GABA binds to two classes of receptors, ionotropic $GABA_A$ receptor and metabotropic $GABA_B$
50 receptor. Interestingly, both types of GABA receptors have been found on HSPCs. GABA type A
51 receptor subunit rho 1 (GABRR1) marks a subset of HSPCs and its deletion inhibited
52 megakaryocyte differentiation and reduced blood platelets (Zhu et al., 2019). In our previous work,
53 we showed that loss of GABA type B receptor subunit 1 (GABBR1) reduced proliferation and
54 reconstitution capacity of hematopoietic stem cells (HSCs), and impaired B cell production (Shao
55 et al., 2021). While these findings suggest GABA has a pleiotropic role in regulating HSPC activity,
56 the sources of GABA in the BM remain unclear. We examined the spatial distribution of GABA in
57 the BM using imaging mass spectrometry and found it was enriched in the endosteal region of the
58 mouse femur (Shao *et al.*, 2021). GABA production is catalyzed by glutamate decarboxylases 1

59 and 2 (GAD1/2) (Erlander et al., 1991). Work by us and others showed *GAD1* but not *GAD2* is
60 expressed in human and mouse B cells that are also enriched for GABA metabolite (Shao et al.,
61 2021, Zhang et al. 2021). We sought to block GABA production from various BM niche cell types.
62 We show that B cells and endothelial cells produce GABA, which is required for the maintenance
63 of the HSPC pool. HSPCs are primed to commit to the B cell lineage when GABA level in the
64 microenvironment is low. We propose that GABA serves as an environmental cue to regulate the
65 decision between HSPC proliferation and B cell production to maintain homeostasis of the B cell
66 pool.

67

68 **Results**

69 *B cells are a source of GABA in the bone marrow niche*

70 To determine if B cells are an autonomous source of GABA, we tracked GABA production
71 throughout B cell development using the OP9 stromal cell co-culture system (Holmes and Zuniga-
72 Pflucker, 2009; Shao *et al.*, 2021). In brief, HSPCs (Lin-/c-Kit+/Sca-1+) sorted from wild-type
73 (WT) mice were co-cultured with stromal cells and examined at 3-day intervals. GABA level in
74 the co-culture media was determined by mass spectrometric analysis, and B lineage cell production
75 was determined by flow cytometry (Fig. 1A-B). We found Cd19+ cells emerged on Day 9 and
76 underwent rapid expansion in the following three days (Fig. 1A-C). Our baseline was GABA level
77 in media and OP9 cells alone that do not produce GABA, to normalize against the small amount
78 of GABA present in fetal bovine serum. During B cell differentiation the GABA level remained
79 low until Day 9 and then increased dramatically at Day 12 (Fig. 1C). The synchronization of B
80 lineage cell emergence and GABA production demonstrated B cells are a source of GABA. This

81 autonomous production of GABA by B cells during differentiation was consistent with the results
82 of others that detected GABA in B cells purified from human peripheral blood and mouse lymph
83 nodes (Zhang et al., 2021).

84 To confirm the *in vivo* functional requirement of GABA production by B cells in the BM niche,
85 we generated mouse models with B cell-specific deletion of *Gad1/2*. We crossed *Cd19-Cre*
86 (Rickert et al., 1997) and *Gad1/2*$^{fl/fl}$*;Rosa26*^{tdTomato} mouse lines (Meng et al., 2016) to generate
87 *Cd19-cre;Gad1/2*$^{fl/fl}$*;Rosa26*^{tdTomato} (Fig. 1D). *Cd19-Cre* activity was shown by the percentage of
88 double positive Cd19+/tdTomato+ cells (Fig. S1A). We isolated HSPCs from *Cd19-*
89 *cre;Gad1/2*$^{fl/fl}$*;Rosa26*^{tdTomato} mice and induced their differentiation into B cells using the OP9 co-
90 culture system. There was significant reduction of GABA level in co-cultures seeded with HSPCs
91 from *Cd19-cre;Gad1/2*$^{fl/fl}$*;Rosa26*^{tdTomato} mice (Fig. 1E).

92 We used mass spectrometry to measure GABA levels in femurs from *Cd19-*
93 *Cre;Gad1/2*$^{fl/fl}$*;Rosa26*^{tdTomato} mice but did not find a significant difference compared to controls
94 (Fig. 1F). Consistent with previously published results that used the B lineage-specific conditional
95 *Gad1* knockout model *Mb1-Cre;Gad1*$^{fl/fl}$ (Zhang *et al.*, 2021), we also observed no change in BM
96 HSPC numbers, number of BM B220+ cells, or percentage of BM and peripheral blood (PB)
97 B220+ cells (Fig. S2A-C). Interestingly, we did observe a decrease in the proportion of BM HSPCs
98 (Fig. 1G), a phenotype that was not tested in the *Mb1-Cre;Gad1*$^{fl/fl}$ model (Zhang *et al.*, 2021),
99 suggesting B cell-derived GABA may directly regulate HSPCs.

100 <u>*Endothelial cells are a source of GABA in the bone marrow niche*</u>

101 Data from our group and others found BM endothelial cells (BMECs) express *Gad1* and are
102 therefore a potential source of GABA (Shao *et al.*, 2021; Zhu *et al.*, 2019). Notably, published

103 mouse BM stroma single cell RNA-seq datasets do not show *Gad1* expression in any populations
104 (Baryawno et al., 2019), while quantitative PCR and bulk RNA-seq detect its expression in B cells
105 and BMECs (Shao *et al.*, 2021; Zhang *et al.*, 2021; Zhu *et al.*, 2019), suggesting *Gad1* transcript
106 may be expressed at low levels. To functionally test if ECs contribute to GABA production in BM,
107 we generated an endothelial-specific *Gad1/2* deletion by crossing *Cdh5-CreERT2* (Sörensen et al.,
108 2009) and *Gad1/2*$^{fl/fl}$*;Rosa26*^{tdTomato} lines to generate *Cdh5-CreERT2;Gad1/2*$^{fl/fl}$*;Rosa26*^{tdTomato}
109 mice (Fig. 2A). Tamoxifen was administered at 5-6 weeks and experiments were performed at 8-
110 12 weeks. *Cdh5-CreERT2* activity was confirmed by the presence of tdTomato+ cells in the BM
111 (Fig. S1B). There was no significant decrease in GABA levels in
112 *CreERT2;Gad1/2*$^{fl/fl}$*;Rosa26*^{tdTomato} BM (Fig. 2B); however, there was a reduction in both number
113 and proportion of HSPCs (Fig. 2C). No change was detected in BM cellularity, CLPs or B cells,
114 or PB myeloid or B cells (Fig. S2D-H). These results demonstrated that *Gad1/2* deletion from
115 BMECs did not broadly impact BM hematopoiesis or GABA levels, however it was sufficient to
116 modulate the proportion and number of HSPCs.

117 <u>Hematopoietic and BMEC-derived GABA coordinates to regulate HSPC activity</u>

118 To understand the contribution of multiple sources of GABA in the BM, we generated a *Tie2-*
119 *Cre;Gad1/2*$^{fl/fl}$*;Rosa26*^{tdTomato} mouse model (Fig. 3A). *Tie2-Cre* is expressed in all ECs during
120 embryonic development and into adulthood (Kisanuki et al., 2001). In the embryo, the hemogenic
121 endothelium gives rise to all definitive HSPCs, meaning in the adult *Tie2-cre* model all ECs and
122 hematopoietic cells have undergone Cre excision (Tang et al., 2010). Therefore, the *Tie2-*
123 *Cre;Gad1/2*$^{fl/fl}$*;Rosa26*^{tdTomato} mouse model enabled us to evaluate the effect of *Gad1/2* deletion in
124 all ECs and hematopoietic cells, inclusive of both B cells and BMECs. Cre activity was confirmed
125 by detection of tdTomato+ cells in the BM (Fig. S1C). We measured GABA levels in the BM of

126 *Tie2-Cre;Gad1/2*$^{fl/fl}$*;Rosa26*^{tdTomato} mice and detected a ~60% reduction compared to control mice
127 (Fig. 3B). Considering that deletion of *Gad1/2* from B cells (Fig. 1F) or ECs alone (Fig. 2B) did
128 not lead to a significant reduction of BM GABA, our results using the *Tie2-Cre* model suggest B
129 cells and BMECs synergize to sustain homeostatic BM GABA levels. As in the EC-specific *Cdh5-*
130 *CreERT2;Gad1/2*$^{fl/fl}$*;Rosa26*^{tdTomato} model (Fig. 2C), we found a decrease in HSPC percentage and
131 number in *Tie2-Cre;Gad1/2*$^{fl/fl}$*;Rosa26*^{tdTomato} BM (Fig. 3C). We did not observe any changes in
132 BM cellularity, CLPs, or B220+ cells, or PB myeloid cells (Fig. S2I-L). We did observe a slight
133 reduction in the percentage of PB B220+ cells (Fig. 3D). Although the *Cd19-Cre*, *Cdh5-CreERT2*,
134 and *Tie2-Cre* models all showed a decrease in the proportion of BM HSPCs, only the combined
135 hematopoietic and EC-specific deletion of *Gad1/2* with *Tie2-Cre* resulted in a significant reduction
136 in BM GABA levels. This shows that GABA is produced by multiple sources at steady state to
137 regulate HSPC activity in the BM niche.

138 <u>Reduced BM GABA levels induced a shift in gene expression profiles of HSPCs</u>

139 To determine if attenuated BM GABA levels result in intrinsic molecular changes in HSPCs, we
140 isolated HSPCs from *Cd19-Cre*, *Cdh5-CreERT2*, and *Tie2-Cre;Gad1/2*$^{fl/fl}$*;Rosa26*^{tdTomato} models
141 and performed bulk RNA-sequencing. Among the total 21,114 genes detected, there were
142 differentially expressed genes (DEGs) in HSPCs of each model when compared to WT: 494 in
143 *Cd19-Cre* (367 upregulated, 127 downregulated); 284 in *Cdh5-CreERT2* (131 upregulated, 153
144 downregulated); 200 in *Tie2-Cre* (73 upregulated, 127 downregulated; FDR < 0.1, |log2FC| > 1;
145 Fig. 4A-B, Fig. S3A). Comparison of DEGs in each mutant showed 21 genes were commonly
146 upregulated upon GABA level reduction, including HSC genes *Hlf*, *Emcn*, and *Fgd5* (Fig. 4A-C)
147 (Calvanese et al., 2022; Engelhard et al., 2024; Gazit et al., 2014; Holmfeldt et al., 2016; Matsubara

148 et al., 2005; Reckzeh et al., 2018; Ueno et al., 2001). Together, this demonstrates that HSPCs
149 respond to changes in GABA produced by BMECs and hematopoietic cells.

150 Our previous analysis of GABA receptor *Gabbr1* loss-of-function mutant HSPCs found they were
151 less proliferative, less responsive to poly(I:C), and had defective B cell differentiation (Shao *et al.*,
152 2021). Intriguingly, phenotypic *Gabbr1* null HSPCs exhibited a shift in transcriptional profiles
153 from undifferentiated progenitor to more B lineage committed progenitor (Shao *et al.*, 2021). We
154 hypothesized loss of *Gabbr1* in HSPCs would simulate attenuated GABA signaling and therefore
155 may mimic HSPCs from a low GABA microenvironment. To test this, we considered DEGs
156 separately in the *Cd19-Cre*, *Cdh5-CreERT2*, and *Tie2-Cre* models and performed gene set
157 enrichment analysis (GSEA) for HSPCs from each model (Fig. 4D,E; Fig. S3C-E; Supplementary
158 Tables). Like *Gabbr1* null HSPCs, we found B cell receptor signaling pathway and B cell
159 activation were enriched in all compared to WT (Fig. S3C-E). We also found interferon signaling
160 pathways were highly upregulated in all *Gad1/2*$^{fl/fl}$ models (Fig 4D). This is consistent with our
161 previous finding that showed a positive correlation between *Gabbr1* expression in HSPCs and the
162 expression of genes related to interferon signaling (Shao *et al.*, 2021), further supporting the
163 GABA-GABBR1 axis in regulating HSPC differentiation and immune response. Consistent with
164 reduced proliferative capacity, E2F and MYC targets, and G2M checkpoint genes were under-
165 represented in *Gad1/2*$^{fl/fl}$ models compared to WT (Fig 4E). Together, this showed that phenotypic
166 HSPCs from a low GABA microenvironment have a similar intrinsic profile to HSPCs that lack
167 GABBR1 receptor signaling.

168 There were many similarities between *CD19-Cre*, *Cdh5-CreERT2*, and *Tie2-Cre* models, however
169 we wanted to consider if there were differences in HSPC regulation that were dependent on the
170 cellular source of GABA. The hierarchical clustering of DEGs from all models showed clusters

171 that were unique to B lineages, BMECs, or both (Fig. 4A). Intriguingly, a curated list of B lineage
172 genes (Miyai et al., 2018) found some of these markers were only strongly upregulated in the
173 *Cd19-Cre* model (e.g., *Cd79a, Cd79b, Vpreb1*; Fig. S3B; Supplementary Tables). *Mecom*, an
174 important regulator of HSCs (Voit et al., 2023), was only upregulated in models that deleted
175 *Gad1/2* from BMECs (i.e., *Cdh5-CreERT2 and Tie2-Cre*). These findings suggest that HSPCs may
176 be differentially regulated by GABA depending on their location in the BM niche, and their
177 proximity to B cells or BMECs. Together, our data shows reduced production of GABA in the BM
178 niche promotes HSPC priming towards B cell lineage commitment, while suppressing HSPC
179 proliferation. Overall, our results reveal a role for GABA as a molecular switch to regulate HSPC
180 activity and B lineage priming.

181

182 **Discussion**

183 GABA is well-known as an inhibitory neurotransmitter in the central nervous system, but it has
184 also been detected in peripheral organs, including the peripheral nervous system, gastrointestinal
185 track, pancreas, and liver (Zhang *et al.*, 2022). In these peripheral tissues, GABA has diverse
186 functions beyond transmitting neural signals, such as regulating immune cell activity in lymph
187 nodes. We demonstrate that GABA serves as an environmental cue in the BM to regulate HSPC
188 differentiation into B cells and maintain the stem cell pool. Despite detectable GABA in multiple
189 peripheral tissues, the sources of GABA remain largely unknown. We show here that B cells and
190 BMECs synergize to maintain homeostatic levels of GABA. Interestingly, GABA level in the BM
191 was not fully reduced even when *Gad1/2* was deleted from both hematopoietic cells and ECs using
192 the *Tie2-Cre* model, suggesting other unknown GABA sources. A survey of published mouse BM
193 stromal cell single cell RNA-seq datasets did not identify any cells that express *Gad1* or *Gad2*

194 (Baryawno *et al.*, 2019), possibly because mRNA expression levels are below the limit of detection
195 using this method. While GAD1 is considered the primary pathway for GABA biosynthesis, other
196 mechanisms have been found, including catalysis of putrescine by aldehyde dehydrogenases (Kim
197 et al., 2015; Li et al., 2025). Further investigation will be needed to identify all the sources of
198 GABA production in the BM microenvironment.

199 HSPCs sorted from the BM of *CD19-Cre*, *Cdh5-CreERT2*, and *Tie2-Cre* models shared many
200 phenotypic similarities. This included an upregulation of immune response genes, including
201 immunoglobulin genes and B cell blueprint genes. This observation was consistent with
202 phenotypic HSPCs sorted from *Gabbr1* null mutant BM, where later-stage B cell commitment
203 genes and pro-B cell-signature genes were highly upregulated (Shao *et al.*, 2021). Strikingly,
204 HSPCs from our *Gad1/2*-deficient BM niche models also had downregulation of genes associated
205 with proliferation, another hallmark of *Gabbr1* null mutant HSPCs. These shared changes in
206 HSPCs that lack the GABBR1 receptor, or reside in BM with lower GABA levels, suggests the
207 GABA-GABBR1 axis is important for balancing a decision between HSPC proliferation and
208 differentiation, specifically towards B lineages.

209 Although we observed many similarities in HSPCs from different *Gad1/2*-deficient BM niche
210 models, there were differences as well, such as B lineage-specific genes *Cd79a*, *Cd79b*, and
211 *Vpreb1* that were uniquely upregulated in *Cd19-cre*$^{+}$*;Gad1/2*$^{fl/fl}$ mutant HSPCs. These
212 transcriptional differences likely arise from the blockade of GABA production in different niche
213 cell types. Spatial mapping of lymphopoiesis in the sternum has revealed that common lymphoid
214 progenitors (CLPs) reside in an arteriolar niche, surrounded by Pre-Pro-B, Pro-B and Pre-B cells
215 (Wu et al., 2024). Within this B cell production line, more lineage-committed cells are located
216 further away from CLPs, suggesting spatial heterogeneity in GABA production. While both

217 endothelial cells and B lineage cells are GABA sources, lymphoid progenitors are proximal to
218 arterioles and more distant from Pro-B and Pre-B cells (Wu *et al.*, 2024). Therefore, the blockade
219 of GABA production from either or both sources could differentially impact HSPC activity
220 depending on their spatial relationships. Understanding the spatial heterogeneity of niche factors
221 will provide more insights into how specialized niches support hematopoiesis.

222 Downstream differentiated hematopoietic cells have been recognized as regulators of their own
223 upstream HSPCs through feedback mechanisms (Kirouac et al., 2010). For example, platelet-
224 biased vWF + HSCs associate with megakaryocyte niches and are regulated by CXCL4 produced
225 by megakaryocytes (Pinho et al., 2018). We demonstrate here that GABA-producing B cells
226 regulate GABBR1+ HSPCs, emphasizing the importance of feedback mechanisms in the BM niche
227 to maintain homeostasis. Pharmacological modulation of these mechanisms could lead to
228 repurposing of clinical neuromodulators to target the hematopoietic and immune systems for
229 therapeutic benefits.

230

231 **Methods**

232 *Mice*

233 Cd19-Cre (JAX stock #006785) (Rickert *et al.*, 1997), *Tie2-Cre* (JAX stock #004128) (Koni et al.,
234 2001), *Gad1*^{lox}*::Gad2*^{lox}*::Rosa26*^{tdTomato} (JAX stock #031800) (Meng *et al.*, 2016), and C57BL/6
235 mice were purchased from the Jackson Laboratory. *Cdh5-CreERT2* was generated by Ralf Adam's
236 group (Sörensen *et al.*, 2009). To generate *Gad1/2* deletion in different cell types, *Cd19-Cre*, *Cdh5-*
237 *CreERT2*, and *Tie2-Cre* were bred to *Gad1*^{lox}*::Gad2*^{lox}*::Rosa26*^{tdTomato}. Genotyping was performed
238 by Transnetyx. At 5-6 weeks of age, *Cdh5-CreERT2;Gad1/2*$^{fl/fl}$ mice or Cre-negative littermate
239 controls were injected with 1.5 mg Tamoxifen (Sigma, T5648; dissolved in medium chain fatty
240 acids (Sigma, C8267)) at 10 mg/mL per day for 5 consecutive days to induce Cre activity. Both
241 male and female mice between 8-12 weeks of age were used in all the studies. All mice were
242 housed in the breeding core at the University of Wisconsin-Madison. All protocols were approved
243 by the University of Wisconsin-Madison Institutional Animal Care and Use Committee.

244 *Flow cytometry of hematopoietic populations*

245 Femurs and tibias were harvested from 8-12 week-old mice and crushed in phosphate-buffered
246 saline (PBS, Corning, 21-040-CV) containing 2% heat inactivated fetal bovine serum with mortar
247 and pestle. PB was collected by cardiac puncture. RBCs were removed by lysis with BD
248 PharmLyse Lysing Buffer (BD Biosciences, 555899). For HSPC isolation, BM cells were pre-
249 enriched for c-Kit+ cells using c-Kit microBeads (Miltenyi Biotec, 130-091-224) and a Midi
250 MACS separator (Miltenyi Biotec, 130-042-301). BM, PB, or c-Kit-enriched cells were then
251 stained for 30 min at 4°C with combinations of antibodies to the following cell surface markers
252 conjugated with different fluorochromes: CD3 (BioLegend, 17A2), CD11b (BioLegend, M1/70),

253 Ter119 (BioLegend, TER119), Gr1 (BioLegend, RB6-8C5), B220 (BioLegend, RA3-6B2), c-Kit
254 (BioLegend, 2B8), Sca-1 (BioLegend, D7), CD127 (BioLegend, SB/199), CD135 (BioLegend,
255 A2F10). HSPC isolation was performed on BD FACSAria and BD FACSDiscover S8 Cell sorters.
256 Data collection was performed on BD LSRII Fortessa and data analysis was performed using
257 FlowJo v10.10.

258 *Mass spectrometric detection of GABA*

259 For LC/MS/MS analysis of GABA, mouse bones were prepared by homogenization, precipitation,
260 and filtration. Details are provided in Supplementary Methods.

261 *In vitro B cell differentiation assay*

262 OP9 stromal cells were purchased from American Type Culture Collection (CRL-2749) and were
263 grown as previously described (Shao *et al.*, 2021). For each experiment, we harvested BM from 1
264 or 2 WT or Gad1/2 KO mice and sorted 4,000 LSK HSPCs into each well of a 12-well plate;
265 replicates are 3 separate wells for each condition. Each well had a monolayer of OP9 cells at 70-
266 80% confluency and 1 ml DMEM medium containing 10% FBS, 5 ng/ml Flt-3L (PeproTech, 250-
267 31L) and 1 ng/ml IL-7 (R&D Systems, 407-ML-005). Experiments were repeated and the results
268 of one representative experiment are shown. After 7 days of co-culturing, hematopoietic cells were
269 mechanically detached, filtered and transferred to fresh OP9 monolayers. Cells were harvested 12
270 days after initial culturing and stained with Cd45 (BioLegend, 30-F11), B220 (BioLegend, RA3-
271 6B2), Cd19 (BioLegend, 6D5) and Cd11b (Biolegend, M1/70) antibodies. Cells were analyzed by
272 brightfield microscopy Nikon ECLIPSE TS2 and flow cytometry. Conditioned media was
273 analyzed by mass spectrometry. Cell counts were determined by hemacytometer. For time course

274 experiments, cells were harvested and analyzed at 3-day intervals after initiation of co-cultures.
275 Flow cytometry analysis was performed using BD LSRII Fortessa and FlowJo v9/10.10.

276 *Bulk RNA-seq library preparation and sequencing*

277 LSK cells from 8-12 week-old wild-type or *Cd19-Cre;Gad1/2*$^{fl/fl}$, *Cdh5-CreERT2;Gad1/2*$^{fl/fl}$, and
278 *Tie2-Cre;Gad1/2*$^{fl/fl}$ models (triplicates for each group) were sorted using BD FACSAria Cell
279 Sorter or BD FACSDiscover S8 Cell Sorter and collected in Trizol LS (Invitrogen). Nuclease-free
280 water was added to adjust the volume to a final ratio of 3:1 for Trizol LS and sample. Samples
281 were stored at -80°C until ready for RNA extraction. Samples were thawed, equilibrated to room
282 temperature, and 100 uL nuclease-free water was added to each sample to reduce the density of
283 aqueous phase. 5PRIME Phase Lock Gel tubes (Quantabio) were used following the manufacturer
284 instructions to separate the aqueous phase. Once the aqueous phase was separated, 25 ug of
285 GenElute-LPA (Sigma, Cat.56575) was added to each sample for RNA precipitation. After adding
286 isopropanol, samples were stored overnight at -20°C for RNA precipitation. The pellet was then
287 washed three times with 75% ethanol, resuspended in 10 uL nuclease-free water, and stored at -
288 80°C until library preparation.

289 RNA samples were quantified, and integrity was examined using Agilent 2100 Bioanalyzer RNA
290 PicoChip. RNA libraries were prepared by UW-Madison Gene Expression Center using Takara
291 SMARTer Stranded RNA v2 Prep Kit - Pico Input Mammalian (Takara Bio). RNA input for library
292 preparation was 1-2.5 ng. The quality of libraries was examined using Agilent 4200 TapeStation.
293 Sequencing was run on an Illumina NovaSeq X Plus single 2x150 bp lane at the UW-Madison
294 Next Generation Sequencing Core.

295 *Bulk RNA-Seq analysis*

296 Raw reads were checked for quality (FastQC v0.12.1) and adapter sequences were trimmed. Reads
297 were mapped to the mouse reference genome GRCm39 using STAR aligner and read counts were
298 normalized using RSEM by the UW-Madison Bioinformatics Resource Core. Low expression
299 genes were filtered, library size was normalized and DGE (Differential Gene Expression) analysis
300 was performed using EdgeR (v4.4.2). Principal component analysis identified an outlier that was
301 removed from further analysis. The final analysis included n=3 samples of sorted HSPCs from WT,
302 *Tie2-Cre;Gad1/2*$^{fl/fl}$, and *Cdh5-CreERT2;Gad1/2*$^{fl/fl}$ BM samples, and n=2 from *Cd19-*
303 *Cre;Gad1/2*$^{fl/fl}$. Pairwise comparisons between WT samples and each mutant were performed using
304 the quasi-likelihood F-test and genes with Log2 Fold Change > 1 and False Discovery Rate (FDR)
305 < 0.1 were selected as DE genes. For heatmaps depicting unsupervised hierarchical clustering,
306 genes that were differentially expressed in at least one mutant were used with the following
307 parameters. GSEA (Gene Set Enrichment Analysis) of HSPCs isolated from mutants was
308 performed using clusterProfiler (release 3.21) with GseaPreranked method. MSigDB Gene sets
309 were downloaded using R package msigdbr (v7.5.1). Gene sets used for GSEA included
310 HALLMARK and GO:BP sets. Rank scores for each pairwise comparison were created by
311 multiplying the negative log of the p-value by the sign of the log fold change and ranking in
312 descending order. A cutoff of adjusted p value < 0.05 was applied for GSEA and results were
313 further filtered using the following criteria: adjusted p-value < 0.01, setSize >= 15 and <= 301,
314 abs(NES) >= 2. Data was submitted to NCBI GEO under the accession number GSE294951.

315 *Statistics*

316 The data was presented as mean ± sd. For the comparison between single experimental and control
317 groups, Welch's t test was used. For comparison between multiple groups, Analysis of Variance
318 (ANOVA) was used, and Tukey's HSD was used as the post-hoc test to determine differences

319 between groups. $P < 0.05$ is considered as statistical significance. GraphPad Prism 10.4 was used

320 for all analyses.

Acknowledgments

The authors thank the University of Wisconsin Carbone Cancer Center Flow Cytometry Laboratory, supported by P30 CA014520, for use of its facilities and services, especially Kathryn Fox and Zach Stenerson for their technical assistance with panel optimization; Kathy Krentz at University of Wisconsin-Madison Animal Models Core for mouse model rederivation and cryopreservation; Megan Latsch and Jody Peter of the University of Wisconsin Biomedical Research Model Services for mouse colony management; Lauren Wells and Sandra Splinter BonDurant at University of Wisconsin-Madison Biotechnology Gene Expression Center (Research Resource Identifier – RRID:SCR_017757) for bulk RNA-sequencing library preparation; University of Wisconsin-Madison Next Gen DNA Sequencing Core for Illumina sequencing; Mark E. Berres at University of Wisconsin-Madison Biotechnology Center Bioinformatics Core Facility (Research Resource Identifier – RRID:SCR_017799) for sequencing reads alignment. Flow cytometry analyses and cell sorting utilized instruments that were supported by the following grants: BD LSR Fortessa (1S10OD018202-01), BD FACS AriaII BSL-2 Cell Sorter, "Jill" (1S10RR025483-01). Research reported in this publication was supported by the Department of Cell and Regenerative Biology at the University of Wisconsin-Madison.

Author contributions

Conceptualization, O.J.T.; Data curation, C.D.; Formal Analysis, C.D., A.E.-B., M.P.H.; Funding Acquisition, O.J.T.; Investigation, C.D., A.E.-B., A.T.S., R.M.C., C.J.O., M.P.H., C.O.S.; Methodology, M.P.H., C.O.S.; Project Administration, O.J.T.; Resources, O.J.T.; Software, C.D.;

Supervision, O.J.T.; Validation, C.D.; Visualization, C.D. and A.E.-B.; Writing - Original draft, C.D.; Writing – reviewing and editing, O.J.T..

Declaration of interests

The authors declare no competing interests.

349 **References**

350 Baryawno, N., Przybylski, D., Kowalczyk, M.S., Kfoury, Y., Severe, N., Gustafsson, K.,
351 Kokkaliaris, K.D., Mercier, F., Tabaka, M., Hofree, M., et al. (2019). A Cellular Taxonomy of the
352 Bone Marrow Stroma in Homeostasis and Leukemia. Cell *177*, 1915-1932 e1916.
353 10.1016/j.cell.2019.04.040.
354 Calvanese, V., Capellera-Garcia, S., Ma, F., Fares, I., Liebscher, S., Ng, E.S., Ekstrand, S., Aguade-
355 Gorgorio, J., Vavilina, A., Lefaudeux, D., et al. (2022). Mapping human haematopoietic stem cells
356 from haemogenic endothelium to birth. Nature *604*, 534-540. 10.1038/s41586-022-04571-x.
357 Engelhard, S., Estruch, M., Qin, S., Engelhard, C.A., Rodriguez-Gonzalez, F.G., Drilsvik, M.,
358 Martin-Gonzalez, J., Lu, J.W., Bryder, D., Nerlov, C., et al. (2024). Endomucin marks quiescent
359 long-term multi-lineage repopulating hematopoietic stem cells and is essential for their
360 transendothelial migration. Cell Rep *43*, 114475. 10.1016/j.celrep.2024.114475.
361 Erlander, M.G., Tillakaratne, N.J., Feldblum, S., Patel, N., and Tobin, A.J. (1991). Two genes
362 encode distinct glutamate decarboxylases. Neuron *7*, 91-100.
363 Gazit, R., Mandal, P.K., Ebina, W., Ben-Zvi, A., Nombela-Arrieta, C., Silberstein, L.E., and Rossi,
364 D.J. (2014). Fgd5 identifies hematopoietic stem cells in the murine bone marrow. The Journal of
365 experimental medicine *211*, 1315-1331. 10.1084/jem.20130428.
366 Holmes, R., and Zuniga-Pflucker, J.C. (2009). The OP9-DL1 system: generation of T-lymphocytes
367 from embryonic or hematopoietic stem cells in vitro. Cold Spring Harbor protocols *2009*,
368 pdb.prot5156. 10.1101/pdb.prot5156.
369 Holmfeldt, P., Ganuza, M., Marathe, H., He, B., Hall, T., Kang, G., Moen, J., Pardieck, J.,
370 Saulsberry, A.C., Cico, A., et al. (2016). Functional screen identifies regulators of murine
371 hematopoietic stem cell repopulation. J Exp Med *213*, 433-449. 10.1084/jem.20150806.
372 Kim, J.I., Ganesan, S., Luo, S.X., Wu, Y.W., Park, E., Huang, E.J., Chen, L., and Ding, J.B. (2015).
373 Aldehyde dehydrogenase 1a1 mediates a GABA synthesis pathway in midbrain dopaminergic
374 neurons. Science *350*, 102-106. 10.1126/science.aac4690.
375 Kirouac, D.C., Ito, C., Csaszar, E., Roch, A., Yu, M., Sykes, E.A., Bader, G.D., and Zandstra, P.W.
376 (2010). Dynamic interaction networks in a hierarchically organized tissue. Molecular systems
377 biology *6*, 417. 10.1038/msb.2010.71.
378 Kisanuki, Y.Y., Hammer, R.E., Miyazaki, J., Williams, S.C., Richardson, J.A., and Yanagisawa, M.
379 (2001). Tie2-Cre transgenic mice: a new model for endothelial cell-lineage analysis in vivo. Dev
380 Biol *230*, 230-242. 10.1006/dbio.2000.0106.
381 Koni, P.A., Joshi, S.K., Temann, U.A., Olson, D., Burkly, L., and Flavell, R.A. (2001). Conditional
382 vascular cell adhesion molecule 1 deletion in mice: impaired lymphocyte migration to bone
383 marrow. J Exp Med *193*, 741-754. 10.1084/jem.193.6.741.
384 Li, L., Kang, Y., Cheng, R., Liu, F., Wu, F., Liu, Z., Kou, J., Zhang, Z., Li, W., Zhao, H., et al.
385 (2025). The de novo synthesis of GABA and its gene regulatory function control hepatocellular
386 carcinoma metastasis. Dev Cell *60*, 1053-1069 e1056. 10.1016/j.devcel.2024.12.007.
387 Liu, Y., Chen, Q., Jeong, H.W., Han, D., Fabian, J., Drexler, H.C.A., Stehling, M., Scholer, H.R.,
388 and Adams, R.H. (2021). Dopamine signaling regulates hematopoietic stem and progenitor cell
389 function. Blood *138*, 2051-2065. 10.1182/blood.2020010419.
390 Matsubara, A., Iwama, A., Yamazaki, S., Furuta, C., Hirasawa, R., Morita, Y., Osawa, M.,
391 Motohashi, T., Eto, K., Ema, H., et al. (2005). Endomucin, a CD34-like sialomucin, marks
392 hematopoietic stem cells throughout development. J Exp Med *202*, 1483-1492.
393 10.1084/jem.20051325.

394 Méndez-Ferrer, S., Lucas, D., Battista, M., and Frenette, P.S. (2008). Haematopoietic stem cell
395 release is regulated by circadian oscillations. Nature *452*, 442-447. 10.1038/nature06685.
396 Meng, F., Han, Y., Srisai, D., Belakhov, V., Farias, M., Xu, Y., Palmiter, R.D., Baasov, T., and Wu,
397 Q. (2016). New inducible genetic method reveals critical roles of GABA in the control of feeding
398 and metabolism. Proc Natl Acad Sci U S A *113*, 3645-3650. 10.1073/pnas.1602049113.
399 Miyai, T., Takano, J., Endo, T.A., Kawakami, E., Agata, Y., Motomura, Y., Kubo, M., Kashima, Y.,
400 Suzuki, Y., Kawamoto, H., and Ikawa, T. (2018). Three-step transcriptional priming that drives the
401 commitment of multipotent progenitors toward B cells. Genes & development *32*, 112-126.
402 10.1101/gad.309575.117.
403 Pinho, S., and Frenette, P.S. (2019). Haematopoietic stem cell activity and interactions with the
404 niche. Nat Rev Mol Cell Biol *20*, 303-320. 10.1038/s41580-019-0103-9.
405 Pinho, S., Marchand, T., Yang, E., Wei, Q., Nerlov, C., and Frenette, P.S. (2018). Lineage-Biased
406 Hematopoietic Stem Cells Are Regulated by Distinct Niches. Dev Cell *44*, 634-641 e634.
407 10.1016/j.devcel.2018.01.016.
408 Reckzeh, K., Kizilkaya, H., Helbo, A.S., Alrich, M.E., Deslauriers, A.G., Grover, A., Rapin, N.,
409 Asmar, F., Gronbaek, K., Porse, B., et al. (2018). Human adult HSCs can be discriminated from
410 lineage-committed HPCs by the expression of endomucin. Blood Adv *2*, 1628-1632.
411 10.1182/bloodadvances.2018015743.
412 Rickert, R.C., Roes, J., and Rajewsky, K. (1997). B lymphocyte-specific, Cre-mediated
413 mutagenesis in mice. Nucleic Acids Res *25*, 1317-1318. 10.1093/nar/25.6.1317.
414 Shao, L., Elujoba-Bridenstine, A., Zink, K.E., Sanchez, L.M., Cox, B.J., Pollok, K.E., Sinn, A.L.,
415 Bailey, B.J., Sims, E.C., Cooper, S.H., et al. (2021). The neurotransmitter receptor Gabbr1
416 regulates proliferation and function of hematopoietic stem and progenitor cells. Blood *137*, 775-
417 787. 10.1182/blood.2019004415.
418 Sörensen, I., Adams, R.H., and Gossler, A. (2009). DLL1-mediated Notch activation regulates
419 endothelial identity in mouse fetal arteries. Blood *113*, 5680-5688. 10.1182/blood-2008-08-
420 174508.
421 Tang, Y., Harrington, A., Yang, X., Friesel, R.E., and Liaw, L. (2010). The contribution of the Tie2+
422 lineage to primitive and definitive hematopoietic cells. Genesis *48*, 563-567. 10.1002/dvg.20654.
423 Ueno, M., Igarashi, K., Kimura, N., Okita, K., Takizawa, M., Nobuhisa, I., Kojima, T., Kitamura,
424 T., Samulowitz, U., Vestweber, D., et al. (2001). Endomucin is expressed in embryonic dorsal aorta
425 and is able to inhibit cell adhesion. Biochem Biophys Res Commun *287*, 501-506.
426 10.1006/bbrc.2001.5587.
427 Voit, R.A., Tao, L., Yu, F., Cato, L.D., Cohen, B., Fleming, T.J., Antoszewski, M., Liao, X., Fiorini,
428 C., Nandakumar, S.K., et al. (2023). A genetic disorder reveals a hematopoietic stem cell regulatory
429 network co-opted in leukemia. Nat Immunol *24*, 69-83. 10.1038/s41590-022-01370-4.
430 Wu, Q., Zhang, J., Kumar, S., Shen, S., Kincaid, M., Johnson, C.B., Zhang, Y.S., Turcotte, R., Alt,
431 C., Ito, K., et al. (2024). Resilient anatomy and local plasticity of naive and stress haematopoiesis.
432 Nature *627*, 839-846. 10.1038/s41586-024-07186-6.
433 Zhang, B., Vogelzang, A., and Fagarasan, S. (2022). Secreted immune metabolites that mediate
434 immune cell communication and function. Trends Immunol *43*, 990-1005.
435 10.1016/j.it.2022.10.006.
436 Zhang, B., Vogelzang, A., Miyajima, M., Sugiura, Y., Wu, Y., Chamoto, K., Nakano, R., Hatae, R.,
437 Menzies, R.J., Sonomura, K., et al. (2021). B cell-derived GABA elicits IL-10(+) macrophages to
438 limit anti-tumour immunity. Nature *599*, 471-476. 10.1038/s41586-021-04082-1.

Zhu, F., Feng, M., Sinha, R., Murphy, M.P., Luo, F., Kao, K.S., Szade, K., Seita, J., and Weissman, I.L. (2019). The GABA receptor GABRR1 is expressed on and functional in hematopoietic stem cells and megakaryocyte progenitors. Proc Natl Acad Sci U S A *116*, 18416-18422. 10.1073/pnas.1906251116.

445 **Figure legends**

446 **Figure 1. B cells are a source of GABA in the bone marrow.**

447 (A) Representative flow plots showing the emergence of B lineage cells in the OP9 co-culture.

448 (B) Schematic of HSPC OP9 B cell differentiation co-culture.

449 (C) Left: Quantification of the percentage of Cd19+ B cells at different timepoints; Right: mass

450 spectrometric quantification of GABA level in the media throughout B cell differentiation.

451 (D) Breeding scheme to generate *Cd19-Cre;Gad1/2*$^{fl/fl}$*;Rosa26*^{tdTomato} mice and control mice.

452 (E) Left: Quantification of B cells produced during differentiation of HSPCs; Right: GABA

453 level in the media from *Cd19-cre;Gad1/2*$^{fl/fl}$*;Rosa26*^{tdTomato} mice and WT mice at Day 12.

454 (F) Mass spectrometric quantification of GABA in *Cd19-cre;Gad1/2*$^{fl/fl}$*;Rosa26*^{tdTomato} and

455 control mouse femur (n = 5 mutants vs n = 5 control).

456 (G) Left: Representative flow plots showing the HSPC gates (Lin-/Sca-1+/c-Kit+); Right:

457 Quantification of LSK cell abundance in *Cd19-cre;Gad1/2*$^{fl/fl}$*;Rosa26*^{tdTomato} mice and

458 control mice (n = 9 mutants vs n = 9 control). Data is represented as mean ± SEM (*p<0.05,

459 **p<0.01, ***p<0.001, ****p<0.0001), Welch's test and one-way ANOVA with Tukey's

460 test were performed.

461 **Figure 2. Bone marrow endothelial cells are a source of GABA in the niche.**

462 (A) Breeding scheme to generate *Cdh5-CreERT2;Gad1/2*$^{fl/fl}$*;Rosa26*^{tdTomato} mice and control

463 mice.

464 (B) Mass spectrometric quantification of GABA in *Cdh5-CreERT2;Gad1/2*$^{fl/fl}$*;Rosa26*^{tdTomato}

465 and control mouse femur (n = 3 mutants vs n = 3 control).

466 (C) Left: Representative flow plots showing the HSPC gates (Lin-/Sca-1+/c-Kit+); Right:
467 Quantification of LSK cell abundance in *Cdh5-CreERT2;Gad1/2*$^{fl/fl}$*;Rosa26*^{tdTomato} mice
468 and control mice (n = 11 mutants vs n = 12 control). Data is represented as mean ± SEM
469 (*p<0.05, **p<0.01), Welch's test was performed.

470 **Figure 3. BMEC and hematopoietic cell-derived GABA synergizes to regulate HSPC activity.**

471 (A) Breeding scheme to generate *Tie2-Cre;Gad1/2*$^{fl/fl}$*;Rosa26*^{tdTomato} mice and control mice.
472 (B) Mass spectrometric quantification of GABA in *Tie2-Cre;Gad1/2*$^{fl/fl}$*;Rosa26*^{tdTomato} and
473 control mouse femur (n = 3 mutants vs n = 3 control).
474 (C) Left: Representative flow plots showing the HSPC gates (Lin-/Sca-1+/c-Kit+); Right:
475 Quantification of LSK cell abundance in *Tie2-Cre;Gad1/2*$^{fl/fl}$*;Rosa26*^{tdTomato} mice and
476 control mice (n = 7 mutants vs n = 7 control).
477 (D) Percentage of B220+ cells in the peripheral blood in *Tie2-Cre;Gad1/2*$^{fl/fl}$*;Rosa26*^{tdTomato}
478 mice and control mice (n = 9 mutants vs n = 9 controls). Data is represented as mean ±
479 SEM (*p<0.05), Welch's test was performed.

480 **Figure 4. Reduction in GABA level induced transcriptional changes in HSPCs.**

481 (A) Heatmap of hierarchical clustering based on differentially expressed genes in *Gad1/2*$^{fl/fl}$
482 mutant models, (|logFC| >1, FDR < 0.1).
483 (B) Venn diagram of genes that were commonly or differentially expressed in *Gad1/2*$^{fl/fl}$ mutant
484 models.
485 (C) Heatmap of the expression level of 21 genes that were commonly upregulated in *Gad1/2*$^{fl/fl}$
486 mutant models.
487 (D) GSEA enrichment plots showing upregulated pathways in *Gad1/2*$^{fl/fl}$ mutant models.

488 (E) GSEA enrichment plots showing downregulated pathways in *Gad1/2*$^{fl/fl}$ mutant models.

489 **Supplementary Figure 1. Genetic knockout efficiency in Gad1/2$^{fl/fl}$ mutants.**

490 (A) Gad1 genetic knockout efficiency shown by the percentage of tdTomato+ CD19+ cells in
491 *Cd19-Cre;Gad1/2*$^{fl/fl}$*;Rosa26*^{tdTomato} mice.

492 (B) Gad1 genetic knockout efficiency shown by the presence of tdTomato+ cells in the whole
493 BM cells in *Cdh5-CreERT2;Gad1/2*$^{fl/fl}$*;Rosa26*^{tdTomato} mice.

494 (C) Gad1 genetic knockout efficiency shown by the percentage of tdTomato+ cells in the whole
495 BM cells in *Tie2-Cre;Gad1/2*$^{fl/fl}$*;Rosa26*^{tdTomato} mice.

496 **Supplementary Figure 2. Hematopoietic profiles of Gad1/2$^{fl/fl}$ mutants.**

497 (A) Total BM cells from 1 femur and 1 tibia in *Cd19-Cre;Gad1/2*$^{fl/fl}$*;Rosa26*^{tdTomato} and control
498 mice (n = 9 mutants vs n = 9 control).

499 (B) Quantification of B220+ cell percentage in the PB in *Cd19-Cre;Gad1/2*$^{fl/fl}$*;Rosa26*^{tdTomato}
500 mice and control mice (n = 3 mutants vs n = 3 control).

501 (C) Quantification of BM B220+ cells in *Cd19-Cre;Gad1/2*$^{fl/fl}$*;Rosa26*^{tdTomato} mice and control
502 mice (n = 9 mutants vs n = 9 control).

503 (D) Total BM cells from 1 femur and 1 tibia in *Cdh5-CreERT2;Gad1/2*$^{fl/fl}$*;Rosa26*^{tdTomato} mice
504 and control mice (n = 12 mutants vs n = 12 control).

505 (E) Quantification of common lymphoid progenitors (CLPs; Lin-/Sca-1-lo/c-Kit-
506 lo/CD127+/CD135+) in *Cdh5-CreERT2;Gad1/2*$^{fl/fl}$*;Rosa26*^{tdTomato} and control mice (n = 6
507 mutants vs n = 6 control).

508 (F) Percentage of B220+ cells in the PB in *Cdh5-CreERT2;Gad1/2*$^{fl/fl}$*;Rosa26*^{tdTomato} mice and
509 control mice (n = 9 mutants vs n = 7 controls).

510 (G) Quantification of BM B220+ cell in *Cdh5-CreERT2;Gad1/2*$^{fl/fl}$*;Rosa26*^{tdTomato} mice and
511 control mice (n = 12 mutants vs n = 12 control).
512 (H) Percentage of CD11b+ cells in the PB in *Cdh5-CreERT2;Gad1/2*$^{fl/fl}$*;Rosa26*^{tdTomato} and
513 control mice (n = 6 mutants vs n = 5 control).
514 (I) Total BM cells from 1 femur and 1 tibia in *Tie2-Cre;Gad1/2*$^{fl/fl}$*;Rosa26*^{tdTomato} mice and
515 control mice (n = 7 mutants vs n = 7 control).
516 (J) Quantification of CLPs (Lin-/Sca-1-lo/c-Kit-lo/CD127+/CD135+) in *Tie2-*
517 *Cre;Gad1/2*$^{fl/fl}$*;Rosa26*^{tdTomato} and control mice (n = 7 mutants vs n = 7 control).
518 (K) Quantification of BM B cell abundance in *Tie2-Cre;Gad1/2*$^{fl/fl}$*;Rosa26*^{tdTomato} mice and
519 control mice (n = 12 mutants vs n = 12 control).
520 (L) Percentage of CD11b+ cells in the PB in *Tie2-Cre;Gad1/2*$^{fl/fl}$*;Rosa26*^{tdTomato} and control
521 mice (n = 9 mutants vs n = 9 control). Data is represented as mean ± SEM (*p<0.05),
522 Welch's test was performed.

523 **Supplementary Figure 3. Gene expression profiles of Gad1/2$^{fl/fl}$ mutants.**

524 (A) Distinct gene expression profiles of WT and *Gad1/2*$^{fl/fl}$ mutant models shown by PCA plot.
525 (B) Heatmap of normalized expression levels of B cell blueprint genes in *Gad1/2*$^{fl/fl}$ mutant
526 models.
527 (C) GSEA result showing top enriched GO terms in *Cd19-Cre;Gad1/2*$^{fl/fl}$*;Rosa26*^{tdTomato}
528 mutants.
529 (D) GSEA result showing top enriched GO terms in *Cdh5-CreERT2;Gad1/2*$^{fl/fl}$*;Rosa26*^{tdTomato}
530 mutants.
531 (E) GSEA result showing top enriched GO terms from *Tie2-Cre;Gad1/2*$^{fl/fl}$*;Rosa26*^{tdTomato}
532 mutants.

Supplementary Methods

Mass spectrometric detection of GABA

All solvents for processing and mass spectometry analysis were Optima LCMS grade from Fischer Scientific (Waltham, MA), unless otherwise noted. Individual bones were weighed and placed in a 2-ml screwcap tube pre-loaded with 2.8mm ceramic beads (Fischer Scientific, Pittsburgh PA). Ice cold 150 mM ammonium bicarbonate (Sigma Aldrich, St. Louis MO) was added (5 mls/gram of tissue) and samples were placed on ice. Samples were then homogenized in an Omni 48-place bead mill homogenizer (Omni International, Kennesaw, GA) set to 6m/sec for 30 sec. Sample homogenization was repeated twice more to fully disrupt bone tissue placing samples on ice between replicates. Following processing 50 µl of bone homogenate was transferred to a 1.7 ml microcentrifuge tube and precipitated with 200 µl ACN/1% formic acid containing internal standard, d_6-g-aminobutyric acid, (CDN resource laboratories Langley, BC). To remove insoluble material the samples were spun in a refrigerated centrifuge at 20,000 xg for 15 mins. The supernatant was filtered in a prewashed 96-well format Sirocco plate (Waters Corp. Milford, MA) into a 1-ml receiver plate according to the manufacturer's protocol. The plate was then dried under nitrogen. Samples were resuspended in 150 ul 1% formic acid for LC/MS/MS analysis. Calibrators (0.75 ng/ml-500 ng/ml) and QC samples for g-aminobutyric acid (Sigma Aldrich, St. Louis MO) were prepared in water, as GABA free bone matrix is not available. The calibrators and QC samples were processed in tandem with unknown samples (addition of ISTD, precipitation and filtration).

For quantitative analysis samples, QCs and calibrators were injected in random order onto a 150 mM Intrada Amino Acid Column (Imtakt, Portland OR) using a Waters Acquity I-Class UPLC system (Waters, Milford MA). The column was held at 60 °C and the flow-rate was 0.500 ml/min.

Analytes were eluted from the column using a gradient. Solvent A was water/0.1% FA and solvent B was ACN/0.1% FA. Briefly, 7.5 µl of sample was injected at 30% B and the %B was ramped to 75% B in 5.5 minutes, then to 99% in 0.2 min. The %B was held at 99% for 1.3 minutes before returning to 30% in 0.2 min followed by a re-equilibration hold at 1.2 minutes before injection of the next samples. Eluate from the column was analyzed in positive ion mode using a QTrap 5500 hybrid triple quadrupole mass spectrometer (SCIEX, Framingham MA) operating in multiple-reaction-mode (MRM) under conditions optimized for detection of the analyte and internal standard. For g-aminobutyric acid the transitions were: parent ion 104.05/product ions 87, 86 and 69. The transitions for d_6-g-aminobutyric acid: parent 110.09/product ions 93, 92.5 and 73.10. All transitions had a 50 msec dwell time. Triplicate injections of samples, calibrators and QCs were used for quantitative analysis allowing calculation of mean and standard deviation, blanks were run between each injection. The mean area under the curve (AUC) of the analyte relative to ISTD was used to construct a quadratic fit for the calibration curve in the MultiQuant software (SCIEX, Framingham, MA). Calibrators were excluded from quantitation models if their calculated concentrations were >15% different from theoretical. For all calibrators, samples, or QCs if the calculated %RSD of the triplicate injections was >15% samples were not considered valid.

All calibration curves had r-values $\geq$ 0.995. For all assays QC samples at each concentration fell within 15% of theoretical concentrations. The lower limit of detection was based on a signal to noise value of three (determined in MultiQuant). The lower limit of quantitation for each assay was based on either a signal to noise value of ten, or set at a g-aminobutyric acid concentration equal to the lowest concentration calibrator, whichever was higher. The upper limit of quantitation for each assay was set at the highest calibrator meeting the $\pm$15% of theoretical metric.

Graphical Abstract

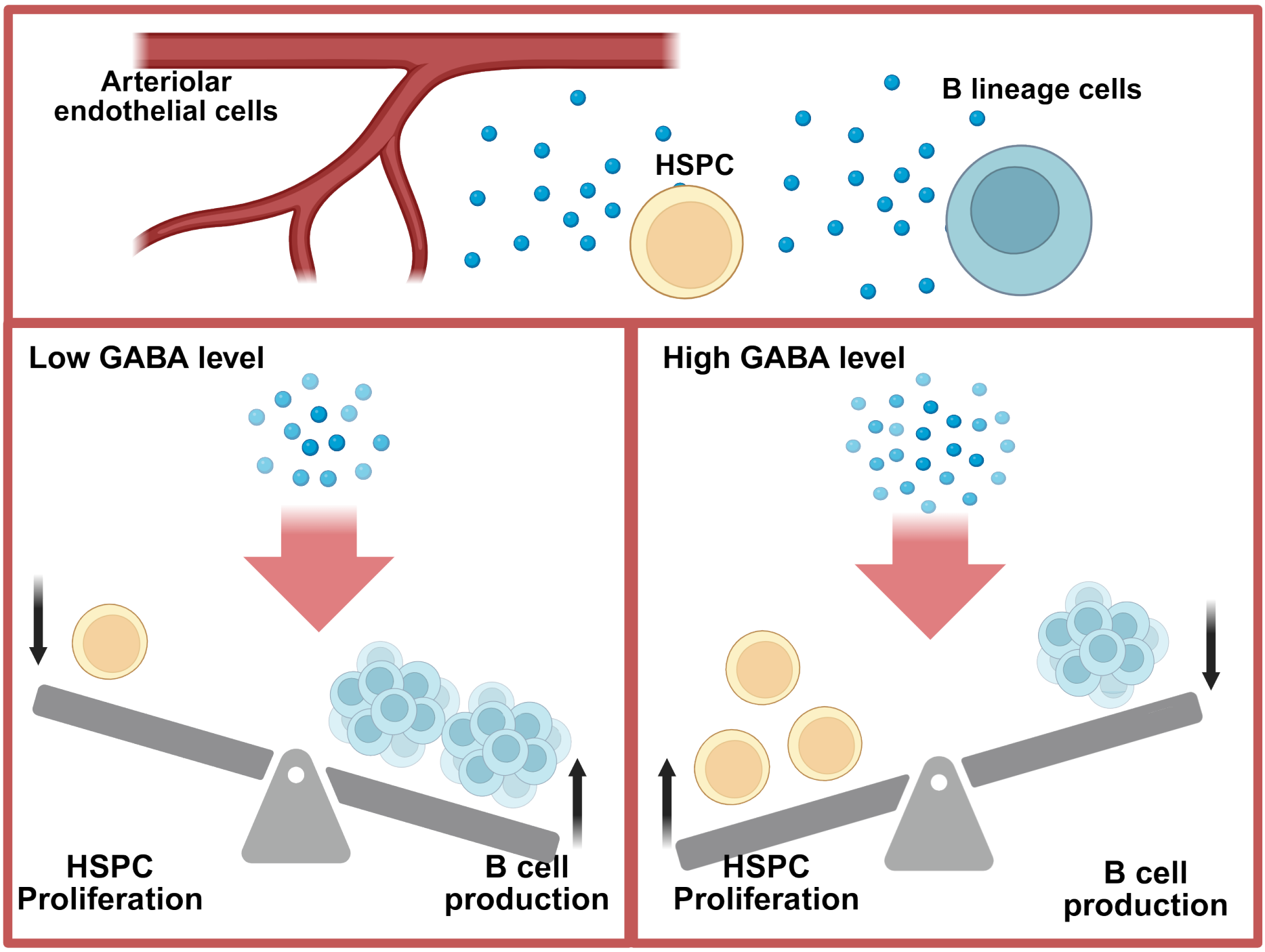

Figure 1

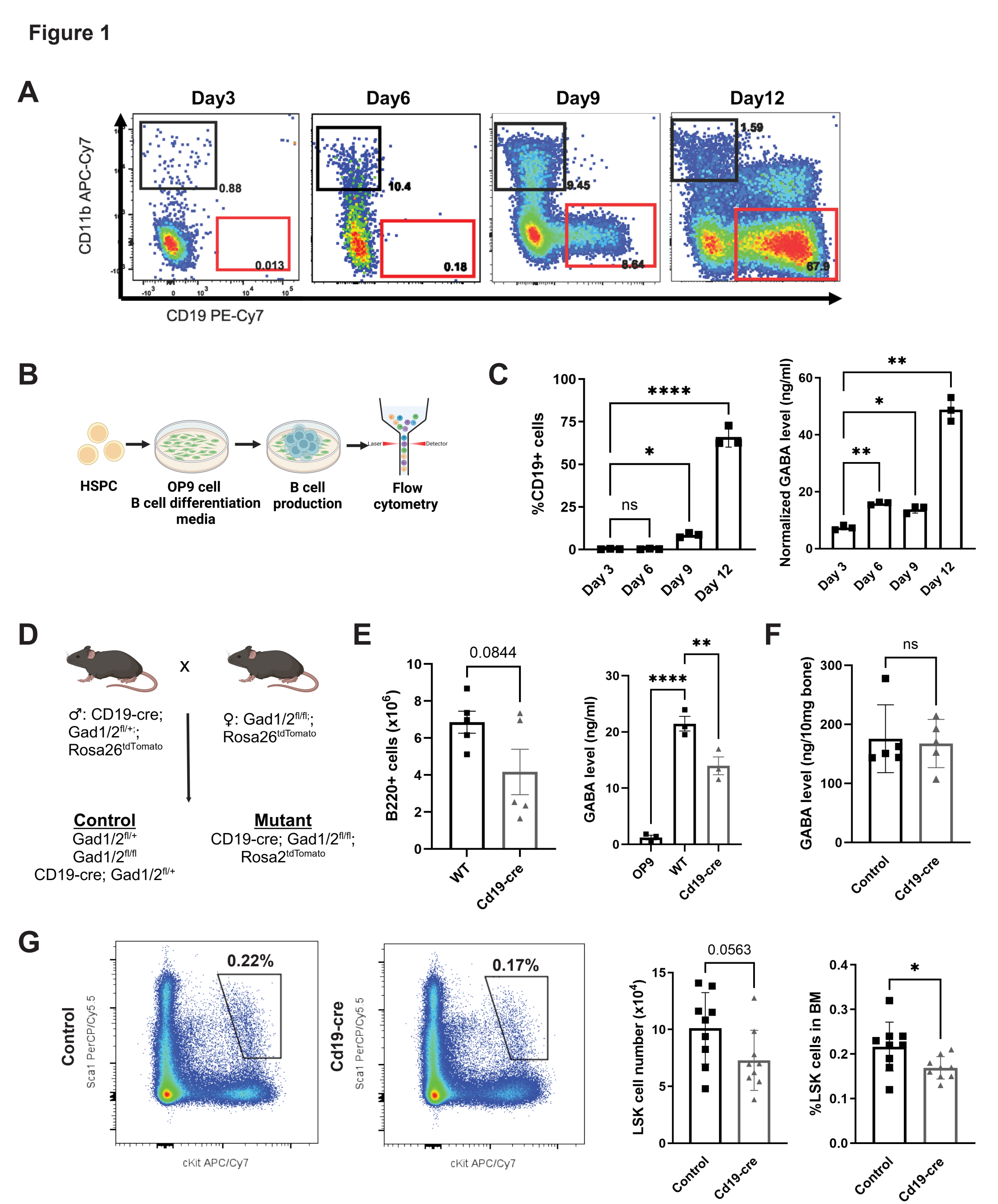
A
Day3
Day6
Day9
Day12
CD11b APC-Cy7
CD19 PE-Cy7
0.88
0.013
10.4
0.18
9.45
8.64
1.59
67.9
B
HSPC
OP9 cell
B cell differentiation media
B cell production
Flow cytometry
Laser
Detector
C
%CD19+ cells
Day 3
Day 6
Day 9
Day 12
ns
*
****
Normalized GABA level (ng/ml)
**
*
D
♂: CD19-cre; Gad1/2fl/+; Rosa26tdTomato
x
♀: Gad1/2fl/fl; Rosa26tdTomato
Control
Gad1/2fl/+
Gad1/2fl/fl
CD19-cre; Gad1/2fl/+
Mutant
CD19-cre; Gad1/2fl/fl; Rosa2tdTomato
E
B220+ cells (x10^6)
0.0844
WT
Cd19-cre
GABA level (ng/ml)
OP9
F
GABA level (ng/10mg bone)
ns
Control
G
Control
Cd19-cre
Sca1 PerCP/Cy5.5
cKit APC/Cy7
0.22%
0.17%
LSK cell number (x10^4)
0.0563
%LSK cells in BM

Figure 2

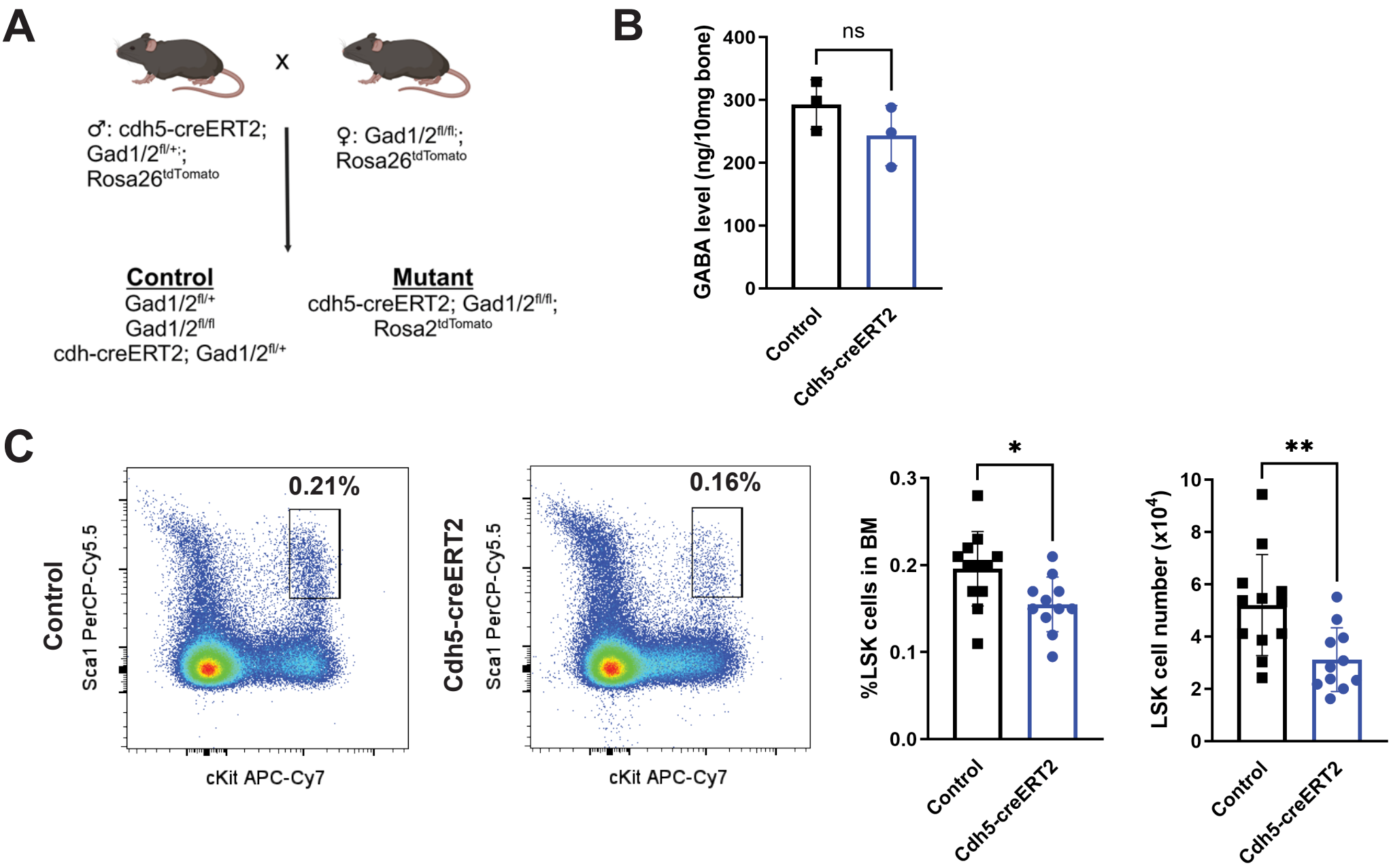
A
x
♂: cdh5-creERT2; Gad1/2fl/+; Rosa26tdTomato
♀: Gad1/2fl/fl; Rosa26tdTomato
Control
Gad1/2fl/+
Gad1/2fl/fl
cdh-creERT2; Gad1/2fl/+
Mutant
cdh5-creERT2; Gad1/2fl/fl; Rosa2tdTomato
B
ns
GABA level (ng/10mg bone)
400
300
200
100
0
Control
Cdh5-creERT2
C
Control
Cdh5-creERT2
Sca1 PerCP-Cy5.5
cKit APC-Cy7
0.21%
0.16%
%LSK cells in BM
0.3
0.2
0.1
0.0
*
LSK cell number (x10^4)
10
8
6
4
2
0
**
Control
Cdh5-creERT2

Figure 3

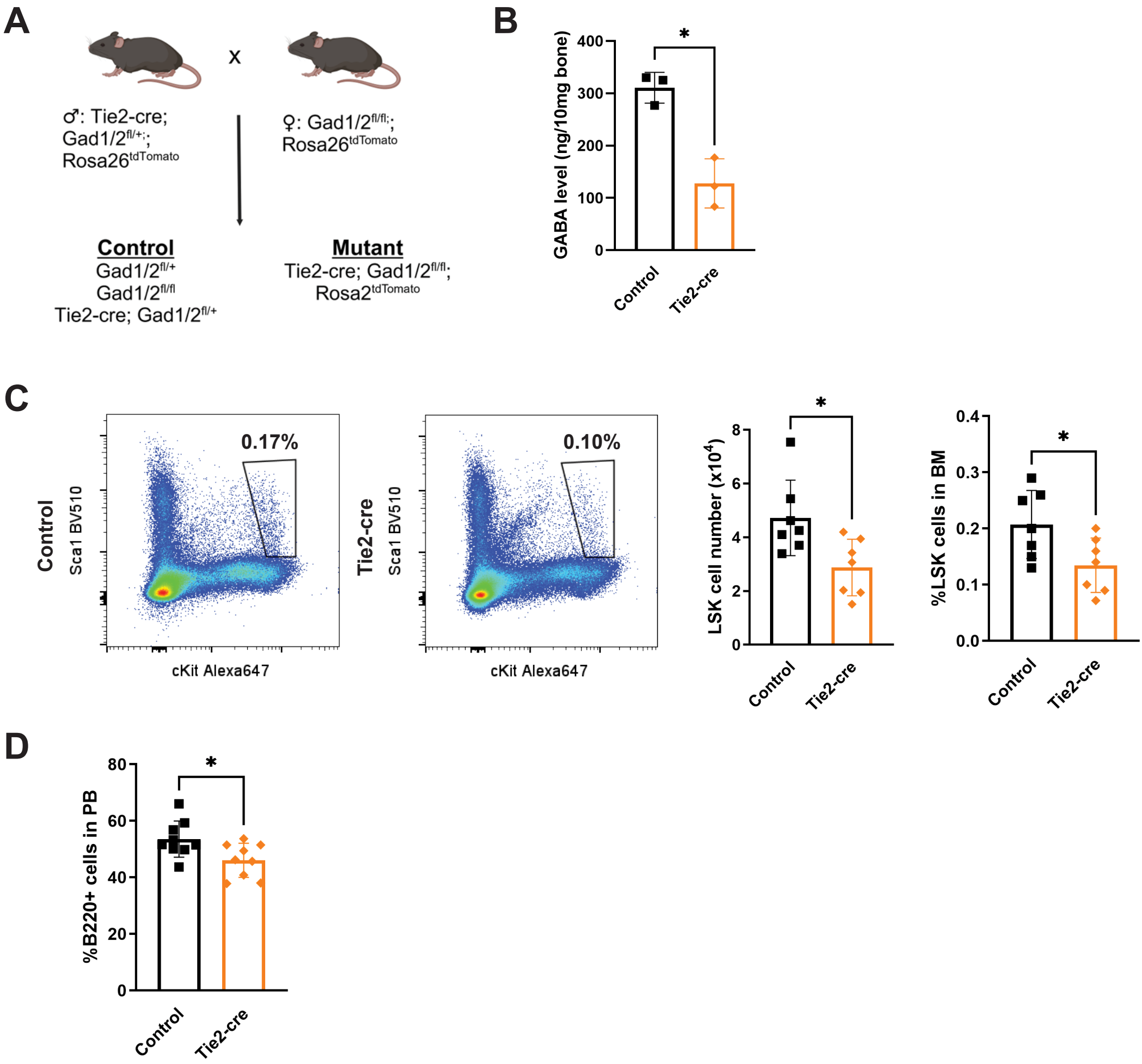
A
x
♂: Tie2-cre; Gad1/2fl/+; Rosa26tdTomato
♀: Gad1/2fl/fl; Rosa26tdTomato
Control
Gad1/2fl/+
Gad1/2fl/fl
Tie2-cre; Gad1/2fl/+
Mutant
Tie2-cre; Gad1/2fl/fl; Rosa2tdTomato
B
GABA level (ng/10mg bone)
400
300
200
100
0
*
Control
Tie2-cre
C
Control
Sca1 BV510
cKit Alexa647
0.17%
Tie2-cre
Sca1 BV510
cKit Alexa647
0.10%
LSK cell number (x10^4)
8
6
4
2
0
*
Control
Tie2-cre
%LSK cells in BM
0.4
0.3
0.2
0.1
0.0
*
Control
Tie2-cre
D
%B220+ cells in PB
80
60
40
20
0
*
Control
Tie2-cre

Figure 4

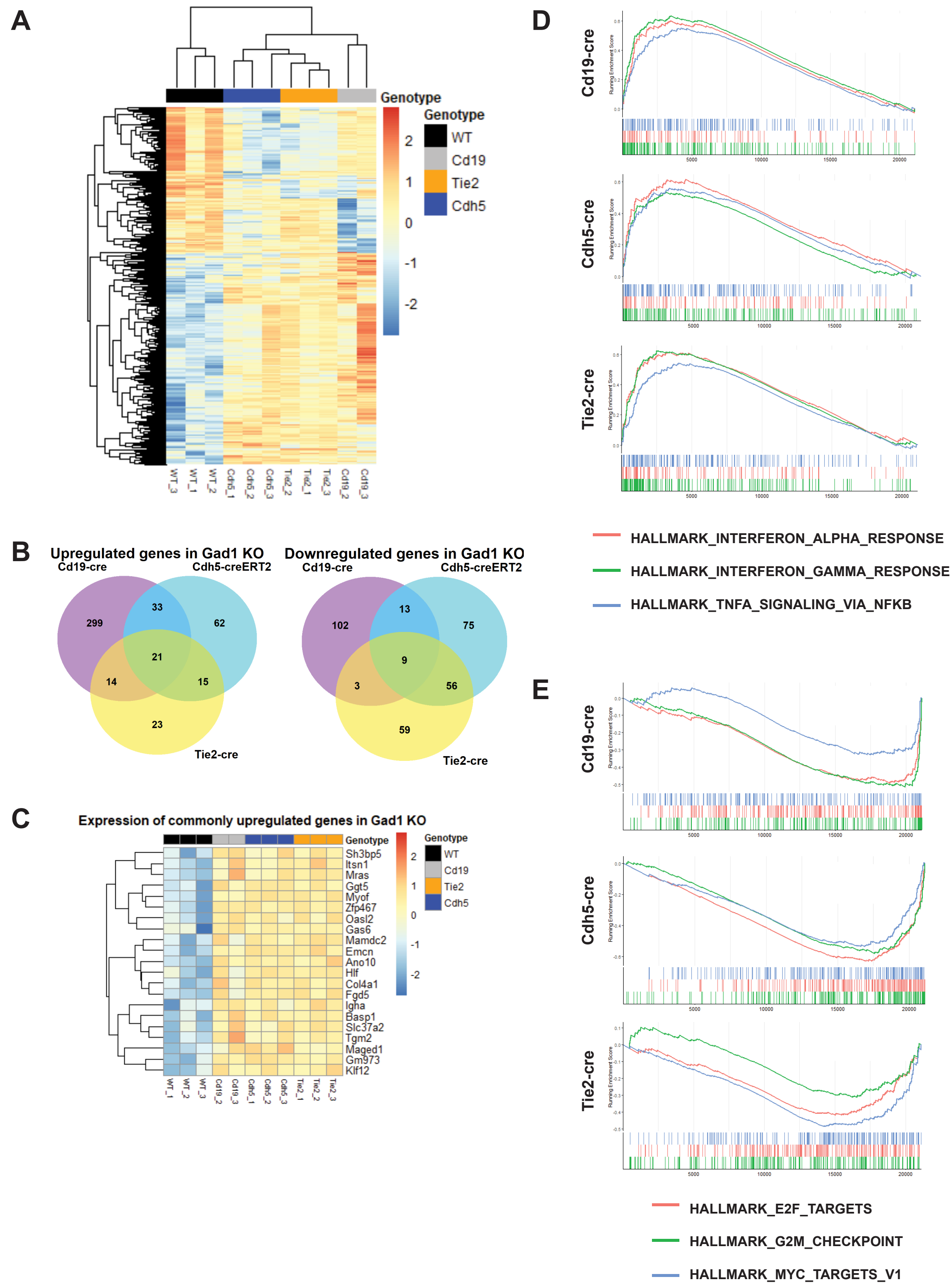
A
Genotype
WT
Cd19
Tie2
Cdh5
2
1
0
-1
-2
WT_3
WT_1
WT_2
Cdh5_1
Cdh5_2
Cdh5_3
Tie2_2
Tie2_1
Tie2_3
Cd19_2
Cd19_3
B
Upregulated genes in Gad1 KO
Cd19-cre
Cdh5-creERT2
Tie2-cre
299
33
62
21
14
15
23
Downregulated genes in Gad1 KO
Cd19-cre
Cdh5-creERT2
Tie2-cre
102
13
75
9
3
56
59
C
Expression of commonly upregulated genes in Gad1 KO
Sh3bp5
Itsn1
Mras
Ggt5
Myof
Zfp467
Oasl2
Gas6
Mamdc2
Emcn
Ano10
Hlf
Col4a1
Fgd5
Igha
Basp1
Slc37a2
Tgm2
Maged1
Gm973
Klf12
D
Cd19-cre
Cdh5-cre
Tie2-cre
Running Enrichment Score
HALLMARK_INTERFERON_ALPHA_RESPONSE
HALLMARK_INTERFERON_GAMMA_RESPONSE
HALLMARK_TNFA_SIGNALING_VIA_NFKB
E
Cd19-cre
Cdh5-cre
Tie2-cre
HALLMARK_E2F_TARGETS
HALLMARK_G2M_CHECKPOINT
HALLMARK_MYC_TARGETS_V1

Supplementary Figure 1

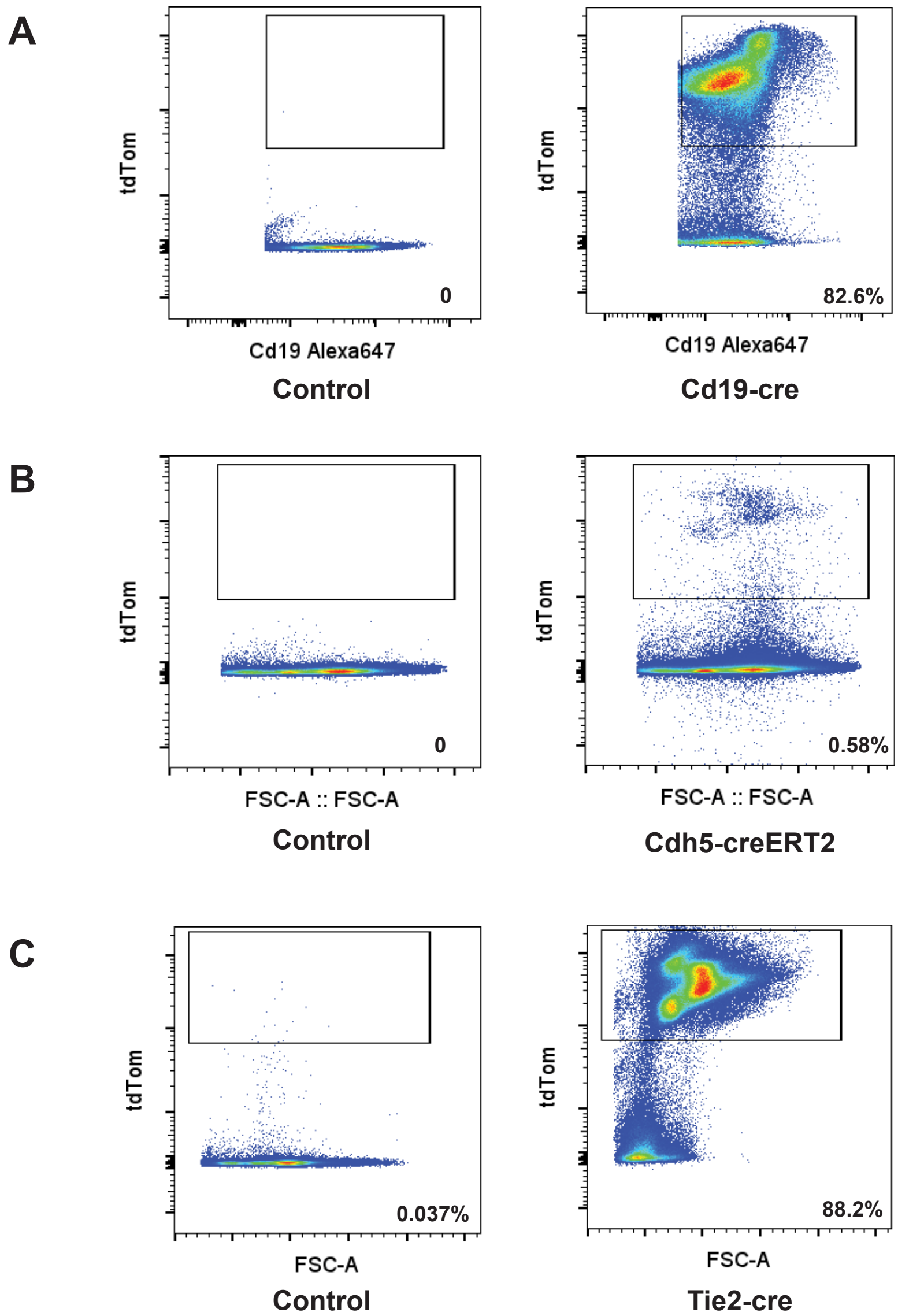

Supplementary Figure 2

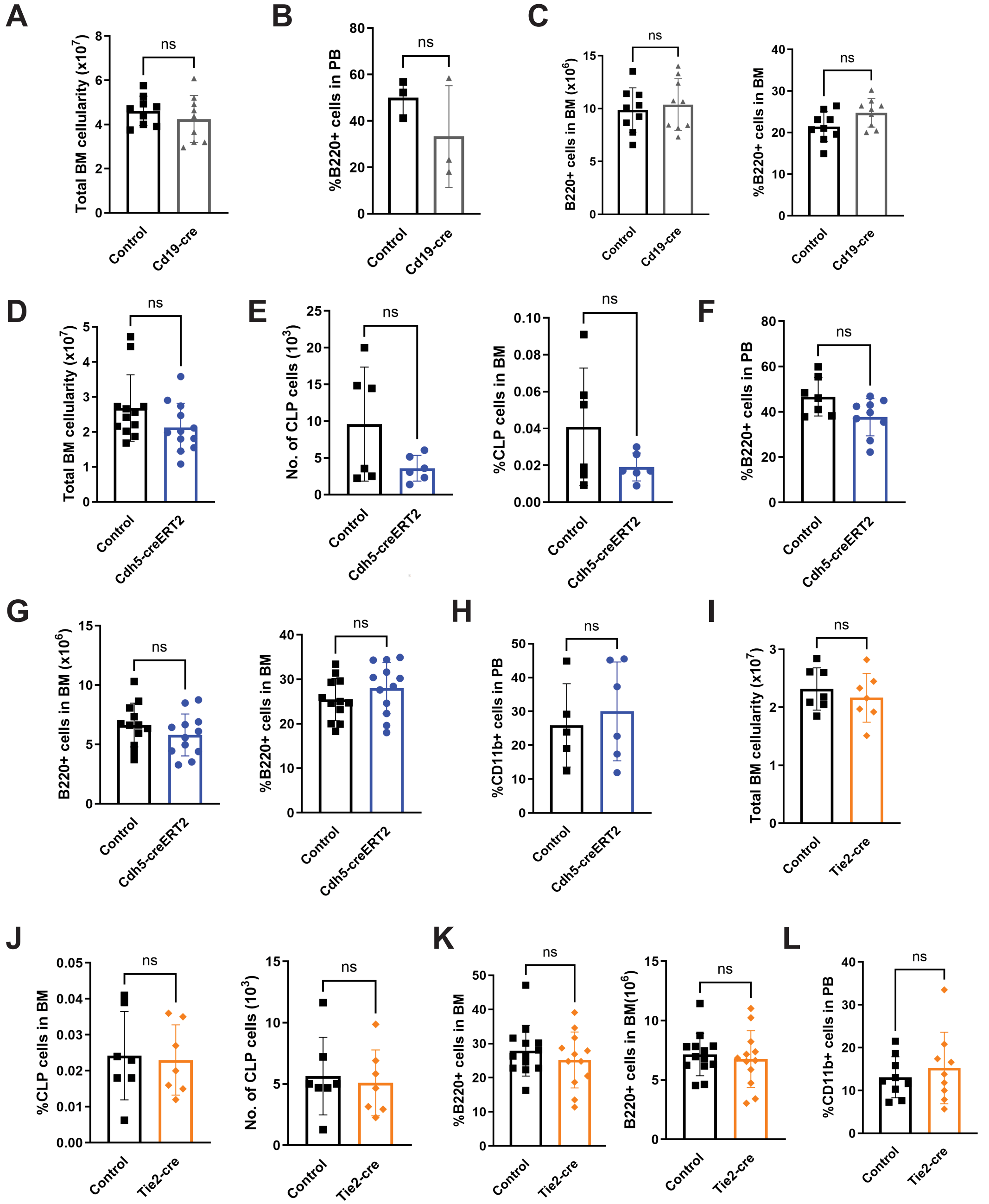

Supplementary Figure 3

A

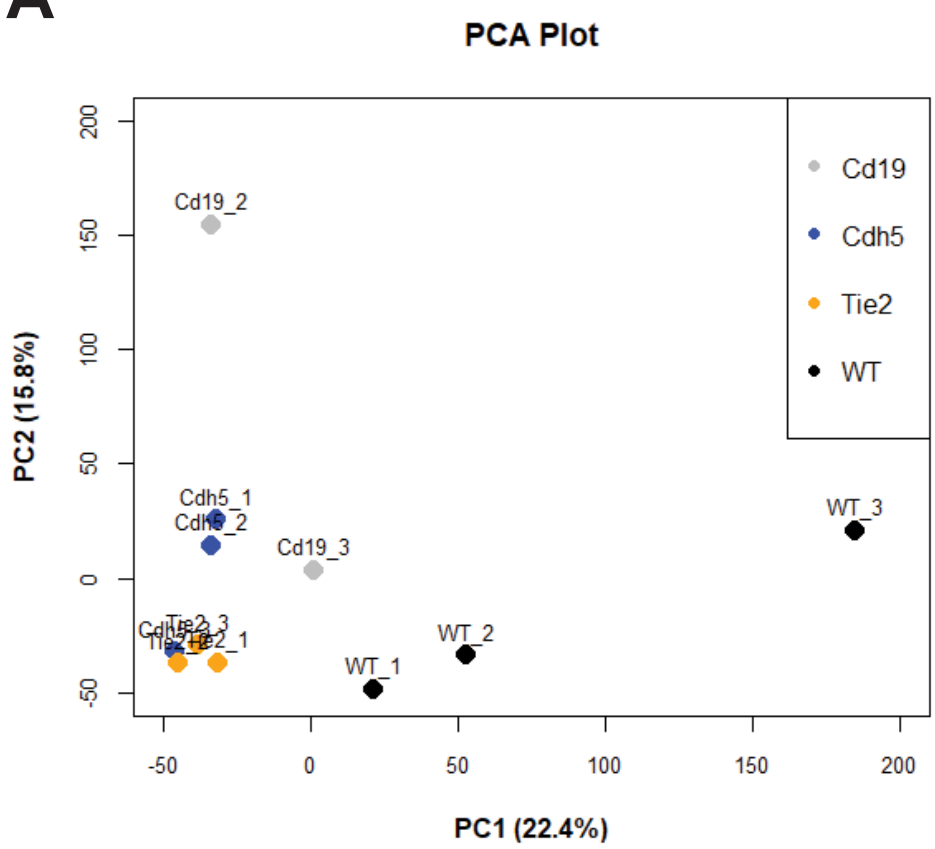

C

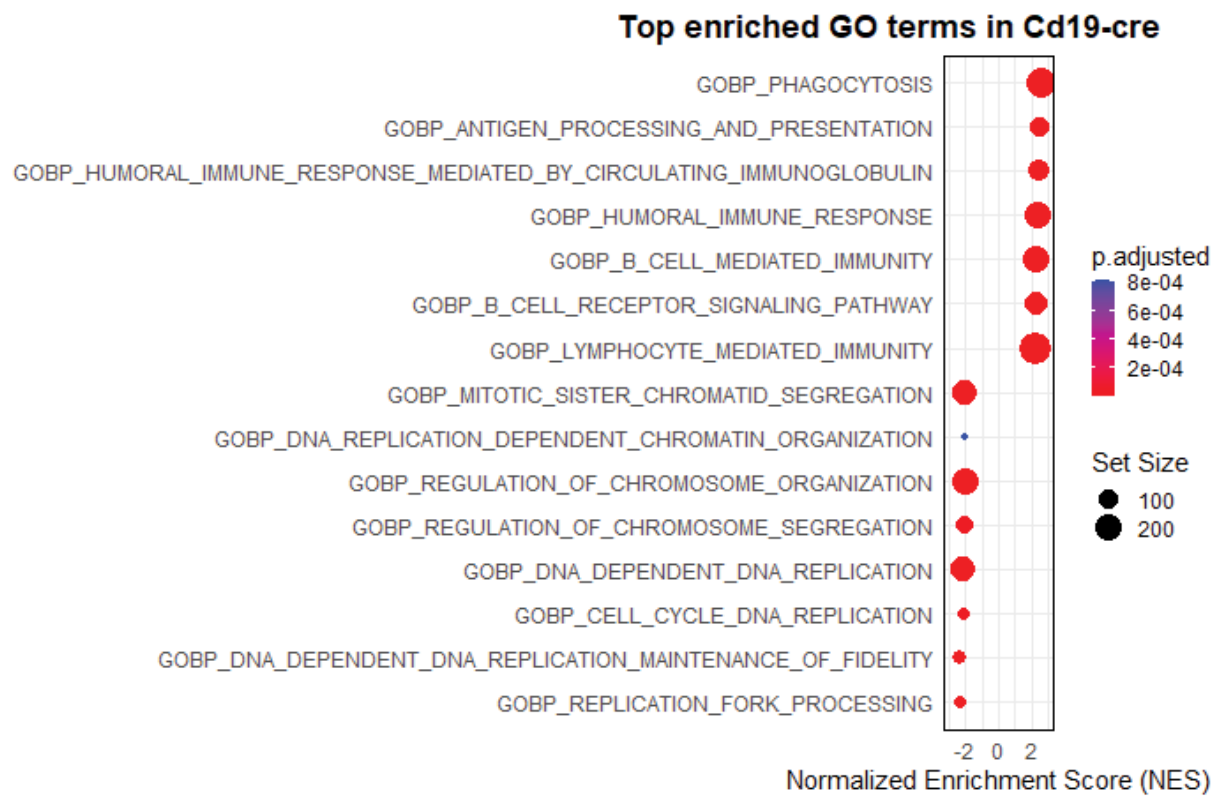

B

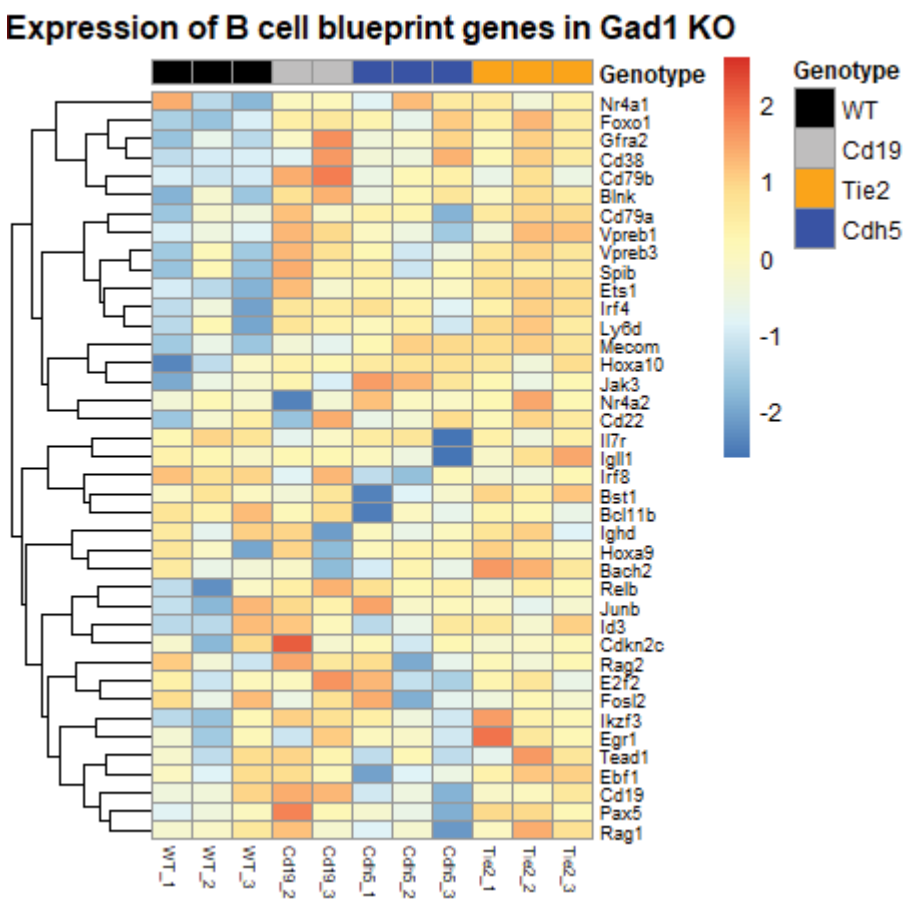

D

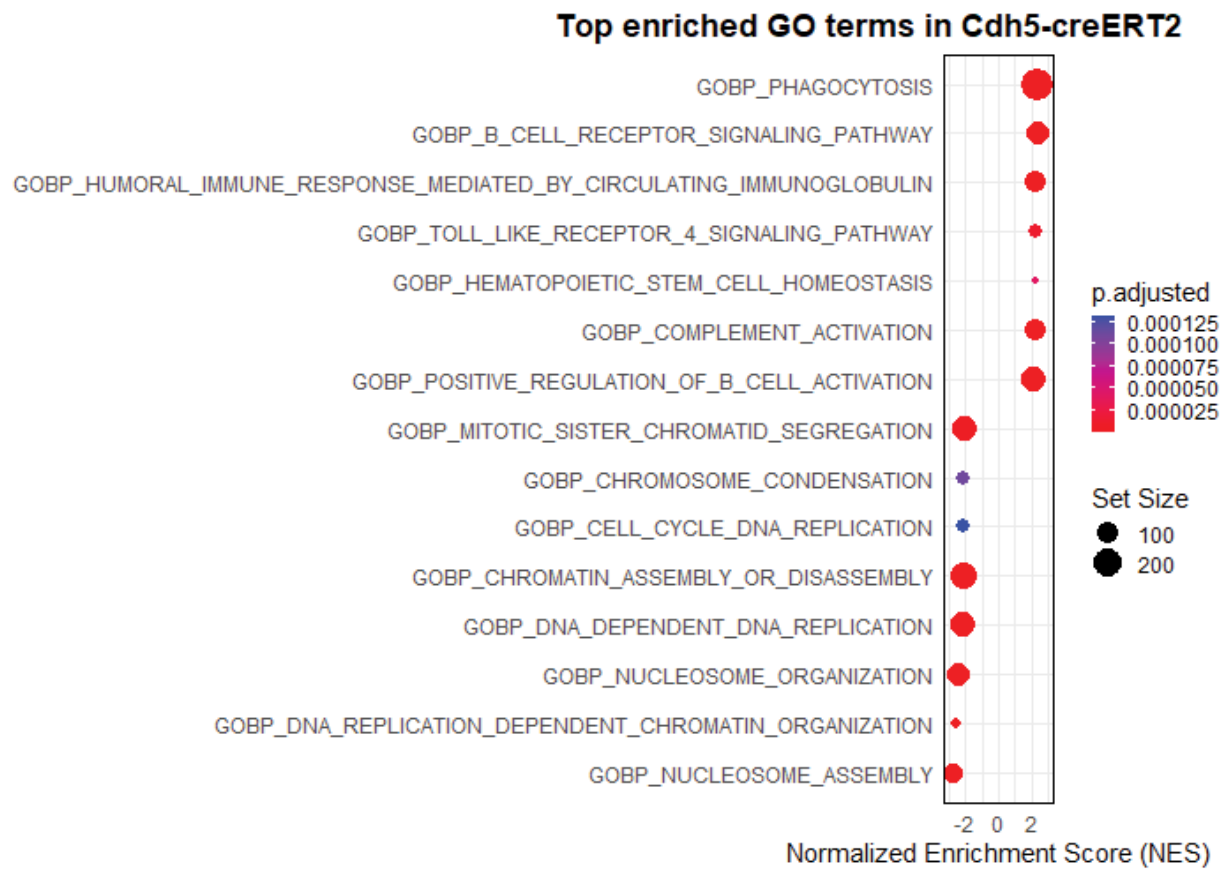
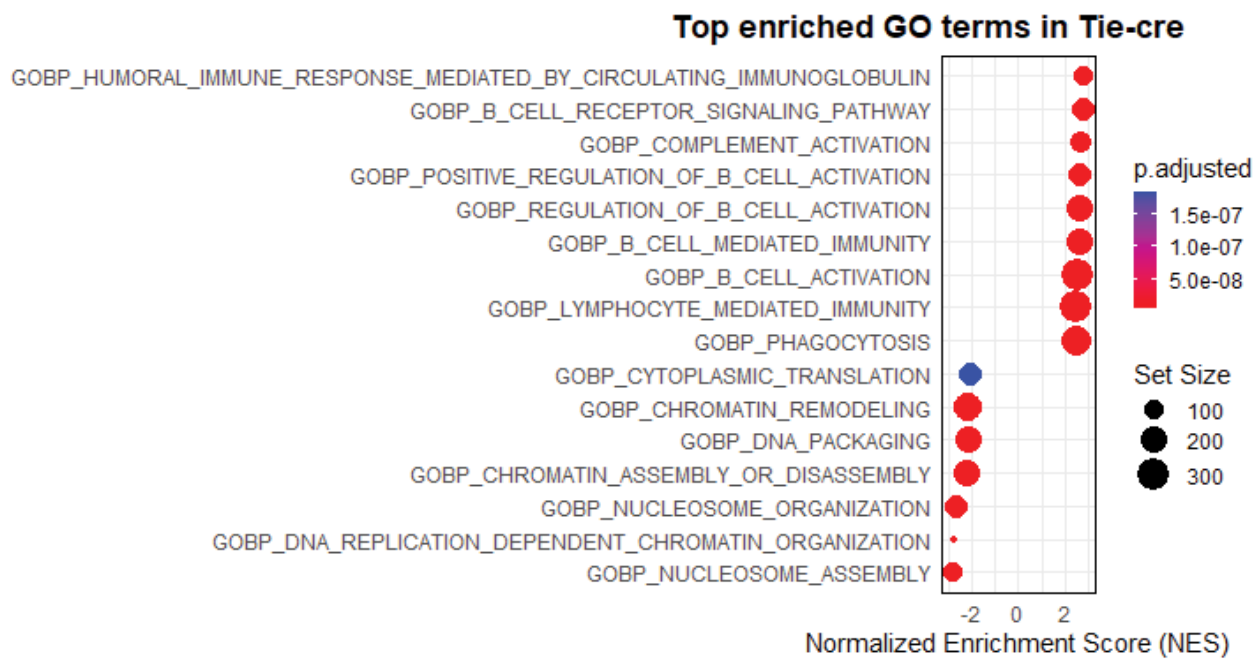
E